

DecoSurf: Recursive Geodesic Patterns on Triangle Meshes

GIACOMO NAZZARO, Sapienza University of Rome, Italy

ENRICO PUPPO, University of Genoa, Italy

FABIO PELLACINI, Sapienza University of Rome, Italy



Fig. 1. Models decorated with *DecoSurf* (large images) to match the style of real-world photographs (upper insets), together with the input meshes (lower insets: teapot 1.5M triangles, elephant 2M triangles). We model decorations by recursively splitting a surface into progressively finer regions, to which we apply material and displacement variations. All patterns were constructed with only four operators that split regions along the isolines or integral curves of scalar fields derived from geodesic computations. Photos of real objects: teapot by Natalya Sots; elephant by Dayal J. Daryanani.

In this paper, we show that many complex patterns, which characterize the decorative style of many artisanal objects, can be generated by the recursive application of only four operators. Each operator is derived from tracing the isolines or the integral curves of geodesics fields generated from selected seeds on the surface. Based on this formulation, we present an interactive application that lets designers model complex recursive patterns directly on the object surface, without relying on parametrization. We support interaction on commodity hardware on meshes of a few million triangles, by combining light data structures together with an efficient approximate graph-based geodesic solver. We validate our approach by matching decoration styles from real-world photos, by analyzing the speed and accuracy of our geodesic solver, and by validating the interface with a user study.

CCS Concepts: • **Computing methodologies** → **Graphics systems and interfaces**; **Shape modeling**.

Authors' addresses: Giacomo Nazzaro, Sapienza University of Rome, Rome, Italy, nazzaro@di.uniroma1.it; Enrico Puppo, University of Genoa, Genoa, Italy; Fabio Pellacini, Sapienza University of Rome, Rome, Italy.

2020. XXXX-XXXX/2020/7-ART \$15.00
<https://doi.org/10.1145/nnnnnnn.nnnnnnn>

Additional Key Words and Phrases: user interfaces, geometry processing

ACM Reference Format:

Giacomo Nazzaro, Enrico Puppo, and Fabio Pellacini. 2020. *DecoSurf*: Recursive Geodesic Patterns on Triangle Meshes. 1, 1 (July 2020), 13 pages. <https://doi.org/10.1145/nnnnnnn.nnnnnnn>

1 INTRODUCTION

Many artisanal objects are decorated with complex patterns, consisting of simple basic shapes, like dots, lines and circles organized into nested hierarchies. The complexity of these decorations comes from repetitive structures that appear handmade instead of being arranged geometrically. Artisans create such decorative patterns by recursively splitting regions to add progressively finer details. Fig. 1 shows examples of these *recursive decorative patterns* that are often found in handcrafted Italian ceramics and wood pieces from Indian art. Note how surfaces are decorated both by changing color and material, but also by altering the surface locally, e.g., adding or removing clay in ceramics.

With the advent of 3D printing and the need for personalization, digital modeling of recursive decorative patterns becomes important. Reproducing these patterns with digital sculpting tools may require hours of work by a skilled artist to decorate a single object. The alternative would be to use procedural programs, grammars or node graphs, but such techniques are notoriously hard for non-technical artists and novices. In the research literature, we are not aware of any work specifically addressing this class of patterns.

In this paper, we present *DecoSurf*, a general yet simple framework for modeling recursive decorative patterns. Fig. 1 and Fig. 12 show examples of decorations created with our model that match real-world styles. We obtain our patterns as recursive applications of only four generic operations, each of which splits a region of the surface into smaller regions to generate progressively finer decorations. At each split, we optionally apply material variations and displacement to define the final look. The key insight of our work is that a large class of decorative patterns can be modeled by recursively cutting regions along the isolines and the integral curves of geodesic fields computed from appropriately selected seeds, namely the regions' borders or points sampled within each region. To better integrate our work with designers workflow, we focus on controlling pattern generation using an interactive application, rather than asking artists to write procedural programs or grammars. To reduce repetitive work though, we also support easy-to-use predefined procedural patterns that are integrated into the interactive workflow.

We model patterns directly on surfaces, relying on geodesic distances for three main reasons. First, we want to work directly on the manifold using its intrinsic metric, thus avoiding distortions, discontinuities and topological artifacts, which arise from parametrization and require complex handling during pattern synthesis. Second, the geodesic metric encodes many intrinsic properties of the surface and remains well defined after mesh split, even when applying displacement. This in turn allows us to define a closed algebra of operators that can be applied at will recursively to generate a remarkable variety of decoration styles. Finally, having one metric for all patterns is practical to implement and easier to optimize compared to using a variety of unrelated operators.

We address surfaces represented with fine triangle meshes, similarly to digital sculpting, using roughly a million triangles per surface to ensure that patterns are finely represented and to model displacement precisely. The main challenge is thus to support interactivity for all operations involved in pattern generation. A key point of this work is the careful design of our data structures, which allow us to implement simple algorithms that scale efficiently to highly tessellated meshes. Our patterns depend on two main operations: computation of geodesic distance fields and cutting triangle meshes along isolines and integral curves of these fields. Mesh cutting is relatively straightforward to implement efficiently, while geodesic computations are notoriously expensive to perform. To address this problem we combine data structures with a small footprint together with a fast, graph-based, approximate, geodesic solver that allows for dynamic update and scales very well with mesh complexity.

We have implemented a prototype user interface, which exposes the pattern operators directly. Fig. 8 shows the interface, while the supplemental video demonstrates the use of each operator and the

creation of a complex decoration. While we focus on interactive editing, we also show that our operators can be used procedurally.

We validate how well *DecoSurf* models real-world recursive decorations in three manners. First, we model decorations to match the styles of real-world artisanal objects. We found that we can replicate complex patterns from different styles with ease. Second, we measure the accuracy and speed of our geodesic solver and of the overall editor to show that we can maintain both accuracy and interactivity while modeling. Third, we run a user study where we ask subjects to model complex patterns with our interface and whether those patterns match real-world surfaces. The main results of the study are that users can reproduce complex patterns with ease and they find that our patterns match real-world styles.

In summary, all these results were made possible by a few key technical contributions:

- the definition of a small set of operators, based on computing geodesic fields from appropriate seeds, which can be combined recursively to obtain many intricate decorations;
- the implementation of a fast geodesic solver that is interactive on meshes with millions of triangles, requires no expensive pre-computation, can be updated efficiently upon mesh editing, and is accurate enough at high triangle count;
- the implementation of a user interface to generate recursive decorative patterns that is simple-to-use while allowing the creation of complex decorations;
- the extension of our model to a procedural use;
- the validation of our model by matching real-world photos, testing accuracy and speed, and running a user study.

2 RELATED WORK

Procedural Patterns. Complex patterns may be generated with procedural methods, for which there exists significant literature. The main differences between procedural algorithms depend on the domain in which they perform the synthesis, the control given to designers, and the underlying algorithmic formulation.

Procedural texturing is at the base of most pattern synthesis used both in the literature and in practice. [12] present the basic methods for procedural texturing, which are applied commonly in practical applications. These methods are very general in the patterns that they define, but they all require the user to describe the pattern using either code or visual languages, and pattern generation requires evaluating a function at each point in either 2D textures, or 3D volumes. We differ substantially from this approach in that we generate structured patterns directly on objects' surfaces instead of relying on generating textures that would require a parametrization. Also, recursive patterns cannot be constructed by evaluating a function on each surface location but they require recursive evaluation of the entire pattern.

A second class of methods generates new patterns directly from example images via non-parametric texture synthesis implemented as variations of constrained random sampling, see [34] for a survey, or via neural network and generative adversarial networks, e.g., [31, 36]. While these methods are remarkably reliable for unstructured patterns, they often fail to capture patterns with complex structural properties. Structured recursive patterns, in particular, cannot be

captured by non-parametric synthesis as shown in [28] for the simpler 2D case.

The last class of methods, and the one more closely related to our work, is based on stochastic grammars that recursively split shapes into smaller components. [28] show that group grammars can be used to describe tangle patterns in the 2D domain. Group grammars are extensions of shape grammars popularized for modeling buildings, see [30] for a recent review. Groups grammars have been extended to procedural animation as motion grammars shown in [6]. [21] uses grammar guided by vector fields to place external details on surfaces, but cannot handle recursive patterns. An alternative approach to grammars is to use a custom programming language to express stationary discrete textures, as shown in [22]. Of these works, [28] is closest to ours since it also models recursive patterns. The main differences between the two approaches are that they use ad-hoc operators only suitable to tangle art in 2D, while we propose general operators working on 3D surfaces. Also, we focus on interactive editing, versus building a grammar system. In fact, our method may be considered a super-set of theirs, while none of the images in this paper could have been generated using the formulation in [28].

Geodesics. Broadly speaking, the literature offers three classes of methods for computing geodesic distance fields and paths over surface meshes. A survey can be found in [2], although several more recent methods exist.

Exact methods for polyhedral surfaces stem from the seminal algorithms presented in [23] and [7], which were improved several times in the literature. But even the most recent methods in this line [27] are too slow to support interaction on moderately large meshes.

Graph-based methods provide approximated solutions of polyhedral geodesics, by restricting possible paths to chains of arcs in a graph. A straightforward shortest path computation on the network of edges results in poor distance estimation and wiggly paths. In [4], such paths are improved by computing shortcuts on-the-fly. [19, 20] precompute an extended graph adding Steiner nodes on edges to improve the approximation. Most recent methods in this class [33, 35] precompute a sub-graph of the complete graph connecting all vertices, such that each possible geodesic path can be approximated well with a sequence of paths in such graph. We rely on a simple variation of graph-based methods, discussed in Sec. 4.2, which scales well to large meshes, and can be maintained very easily and efficiently upon mesh refinement.

PDE methods define the geodesic distance problem in terms of partial differential equations [8, 17] and provide results that approximate geodesic distances on a smoothed surface. The Fast Marching Method [17] requires no pre-processing and could be adapted well to local computations and dynamic mesh refinement, but it is overly slow for our needs. A parallel version of FMM has been proposed very recently [3], which greatly improves time performances, yet remaining slower than our approach, with a comparable accuracy. The heat method [8] requires resolving sparse linear systems of the size of the mesh. It can run very efficiently on relatively large meshes by exploiting pre-factorization, but it cannot be extended easily to manage local computations, or dynamic mesh refinement.

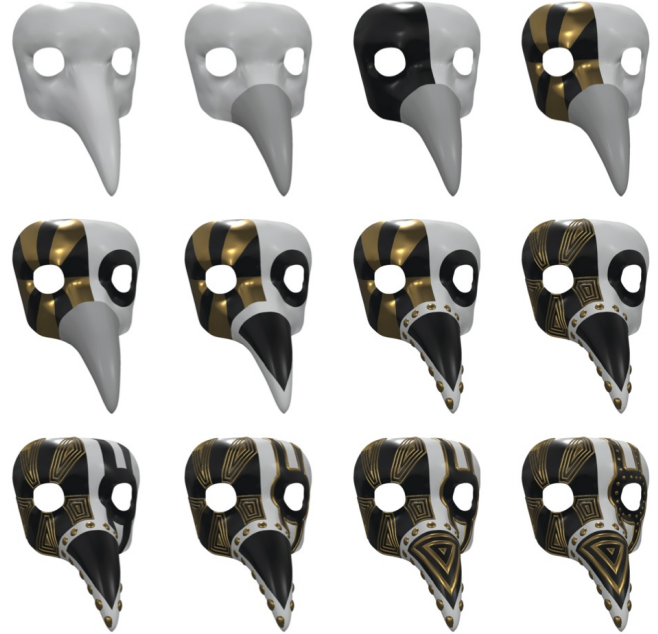


Fig. 2. Complex recursive patterns are obtained in just eleven steps (left to right, top to bottom) starting at a base shape (upper left). At each step we apply a basic operation, which recursively splits the surface into finer decorations. The generated patterns naturally follow the shape of the surface, as they are based on geodesic distance fields.

The former issue can be partially addressed by incorporating the methods proposed in [14, 15].

3 RECURSIVE GEODESIC PATTERNS

We aim at producing patterns defined as recursive subdivisions of a surface into nested shapes. We show that a small arsenal of simple operators, defined upon geodesic fields and combined in the context of a coherent framework, together with the recursive nature of decorative patterns, is sufficient to generate a great variety of patterns that match the style of handmade decorations. Fig. 2 shows an example of a pattern generation sequence.

3.1 Overview

Pattern Representation. Let \mathcal{M} be a 2-manifold, possibly with boundary. A *region* R is a connected subset of \mathcal{M} bounded by a finite number of oriented boundary loops. A *recursive pattern* \mathcal{T} is a tree of regions, having its root at \mathcal{M} and such that the children of each region R in \mathcal{T} form a partition of R . The leaves of \mathcal{T} form a partition of \mathcal{M} and those regions ultimately define the pattern.

Operators. We construct decorative patterns by recursively applying a small set of four operators that split an input region into two or more output regions, by cutting the region with lines or loops. After each split, each region can be assigned a different material, and surface displacement can be optionally applied. In our framework, operators trace lines that are either contour lines of a smooth scalar field f defined over \mathcal{M} , or integral curves of its gradient ∇f .

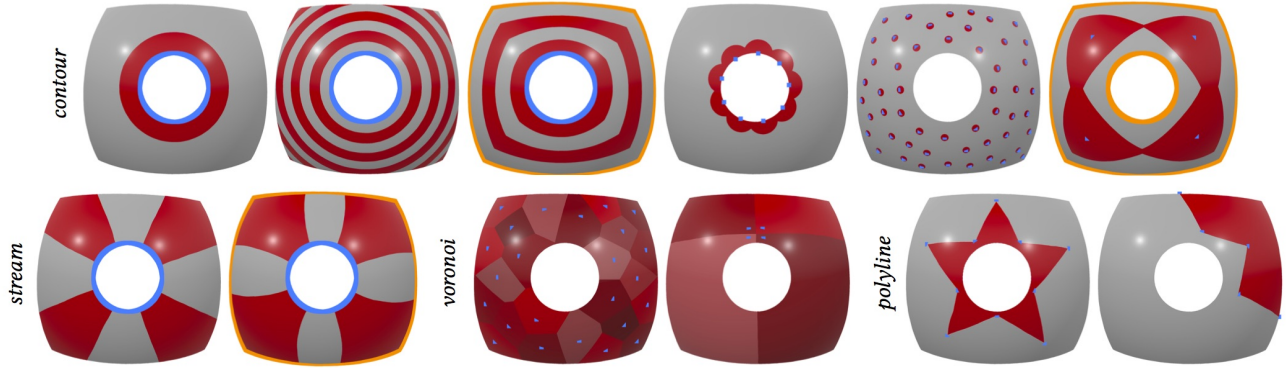


Fig. 3. Example decorations created by applying only one operator with different field and seed sets. (Top, left to right) *Contour* operator with (1) *dist* field from the inner boundary (in blue) cutting along a single isovalue; (2) *dist* field from the inner boundary with multiple isovalues; (3) *blend* field between inner (blue) and outer (orange) boundary, cutting along multiple isovalues; (4) *dist* field from uniform sampling of points along the inner boundary; (5) *dist* field from Poisson sampling of points on the surface; (6) *blend* field between sampled points (blue) and boundaries (orange). (Bottom left, left to right) *Stream* operator with (7) *dist* field from inner boundary; (8) *blend* field between inner and outer boundary. (Bottom middle, left to right) *Voronoi* operator with (9) *dist* field from points selected with Poisson sampling; (10) *dist* field from manually selected points. (Bottom right, left to right) *Polyline* operator with (11) closed polyline on a multiply connected region; (12) open polyline connecting two points on the same boundary loop.

Geodesic metric. We define the scalar field f upon geodesic distances, which depend on both the manifold \mathcal{M} , and a *seed set* S made of points and lines on \mathcal{M} from which distances are computed. Much flexibility of our operators stems from the possibility to set seeds in a proper way, e.g., combining lines from the boundary of a region and points sampled inside a region or on its boundaries.

We consider two types of scalar fields, shown in Fig. 4: the geodesic distance $dist_S(x)$ of surface points x from the seed set S , and the blend between geodesic distance fields from two independent seed sets, defined as

$$blend_{S,S'}(x) = \frac{dist_S(x)}{dist_S(x) + dist_{S'}(x)}.$$

The blend field, already used in [5] to derive parametrizations, has some nice properties: its values are always in the range $[0, 1]$, in particular $blend_{S,S'}(S) = 0$ and $blend_{S,S'}(S') = 1$; and it is anti-symmetric in the sense that $blend_{S,S'}(x) = 1 - blend_{S',S}(x)$. Moreover, if S and S' are lines, its contour lines are parallel to both of them in their vicinity, and the integral curves of its gradient meet them orthogonally.

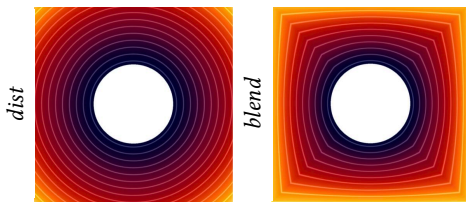


Fig. 4. Field visualization: *dist* field from the center and *blend* field from center to border.

3.2 Operators

In our framework, we use only four operators, which are summarized in Fig. 3 and described in the following.

Contour operator. The *contour* operator traces the contour lines of the geodesic field, either *dist* or *blend*. The generated pattern depends on the selected seeds as well as on an isovalue d . When applied to a region, the contour operator generates two or more regions, splitting the surface with the contour lines at value d . Depending on the selected seeds and the desired isovalue, this operator can be used to construct a variety of patterns. For example, when considering the distance from the region boundary, this operator produces outlines, while if used with points inside a region it produces polka dots. By repeating the cuts at different equally spaced isovalues, the operator generates concentric or parallel stripes, where the density of stripes is controlled with a parameter. The contour operator has been used to obtain most of the decorations on the teapot in Fig. 1 and overall it is the most frequently used operator in all our examples.

Stream operator. The *stream* operator cuts regions by tracing the integral curves of the gradient of the geodesic field, either *dist* or *blend*. In this case, the seed sets are comprised of region boundaries, S and S' , from which the integral lines emanate or end. The generated pattern depends on the selected seeds and the desired number of lines, whose starting points are sampled uniformly along seed S . The stream operator generates n stripes, each bounded by two consecutive integral curves. Such stripes stream outwards S , and towards S' if the latter is specified. The stream operator has been used to obtain the main pattern of the rug on the back of the elephant in Fig. 1, as well as in several parts of the rolling teapot in Fig. 12. Contour and stream operators can be combined to generate grid patterns on cylindrical regions. See the example in Fig. 5 and the paragraph on *Grouping and Hierarchy* below.

Voronoi operator. The *voronoi* operator partitions a region into the cells of a Voronoi diagram in the geodesic metric, each one corresponding to a point in the seed set. The user controls the seeds in the region, which can be either manually selected, or generated with Poisson sampling, as described in Sec. 4.2, to simulate the look of centroidal Voronoi tessellation. Voronoi diagrams are used extensively in procedural pattern generation, but their common use is as a 2D or 3D texture. Our patterns are generated over the surface, so they have a more natural look. We use the Voronoi operator to obtain cellular-like patterns and as a drawing scaffold to place finer details. See examples on the central mask and on the vase to the right in Fig. 10, as well as on the fertility in Fig. 12.

Polyline operator. Finally, the *polyline* operator draws a geodesic polyline on the surface by connecting a sequence of seed points. The polyline splits a region into two if it is closed or it connects two points from the same boundary loop. If instead the polyline connects two different boundary loops, it does not split the region but it is embedded into the region’s boundary and changes its topological type. For instance, two such lines can be used to cut a longitudinal strip from a cylindrical region, e.g., the spout of the teapot in Fig. 1. The polyline operator is most often used to cut large, meaningful patches that are then refined and decorated with the other operators.

3.3 Applying Operators

Seed selection. In our prototype, the user can select region boundaries, either completely or partially, as well as points on the surface. A seed set is made of an arbitrary collection of such selections. Points can be either selected individually, or sampled according to a Poisson distribution in the geodesic metric. Significantly different patterns stem from different selection as already shown in Fig. 3.

Grouping and Hierarchy. To further extend the capabilities of our framework, we support the application of operators not only to the leaves of \mathcal{T} , but also to regions that are higher in the hierarchy. In this case, the operator defines fields and lines in the whole selected region, while all sub-regions that are descendant from it are sliced with such lines, and new leaf regions are generated accordingly. See examples in Fig. 5 and Fig. 9 (grid). This operation is natural in our framework, since field computation and split operators are independent. This same scenario required specialized cutting operations in the group grammars presented in [28]. This extension also implies that we are less sensitive to the order in which operations are applied, a common concern in split grammars [30], thus leaving more freedom to the user.

Perturbation and displacement. We can perturb geodesic fields and displace surface points to obtain a more “handcrafted”, organic, look. Scalar field perturbations simulate the imprecision of artists’ hands; while surface displacement simulates accumulation or removal of material. See examples in Fig. 6 and Fig. 7.

To simulate perturbation and handmade imprecisions, we apply 3D Perlin noise to the vertices of the mesh by offsetting their position along the normal direction before computing geodesic distances. This perturbation is just symbolic and used only by the geodesic solver, while the actual mesh is not changed. Geodesic distances



Fig. 5. (Left) The body of the vase has been partitioned into stripes with a contour operator. (Middle) A Polka dots pattern is obtained with a contour operator applied to Poisson point sampling in each stripe region separately. (Right) The same pattern is applied on the parent region of the stripes, which is the body of the vase; in this case, the whole surface between the red strips is considered as a single piece for point sampling and distance computation.

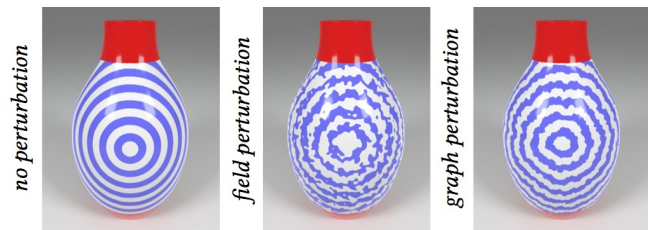


Fig. 6. The same pattern is generated without perturbation, with perturbation of the scalar field and with perturbation applied to the surface before geodesic field computation. Note how perturbing the surface instead of the resulting geodesic field preserves the topology of the generated regions, e.g., connected components.

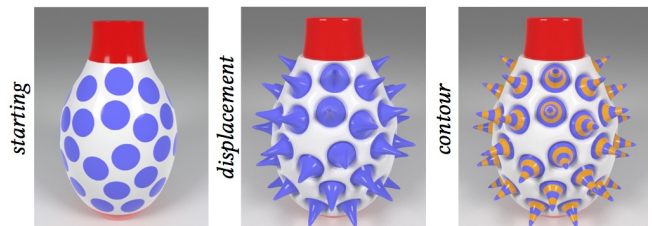


Fig. 7. Example pattern generated applying strong surface displacement using different profiles to create bulges and horn-like structures. Note how we can coherently edit the horns with additional decorations since distance fields are computed on the updated geometry.

computed on such warped geometry are therefore transformed accordingly to a coherent metric and produce irregular shapes, providing organic results. This works significantly better than perturbing the scalar field directly, since this can cause unwanted topological changes to the perturbed regions due to the fact that the perturbed field is no longer a distance field. Perturbation can be controlled by setting the gain and frequency of the Perlin noise. For instance, all the irregular blobs on the body of the teapot in Fig. 1 are actually circles from a perturbed metric; likewise, the irregular stripe patterns on the spherical bodies forming the lid of the same teapot are obtained with perturbation. See also supplemental video.

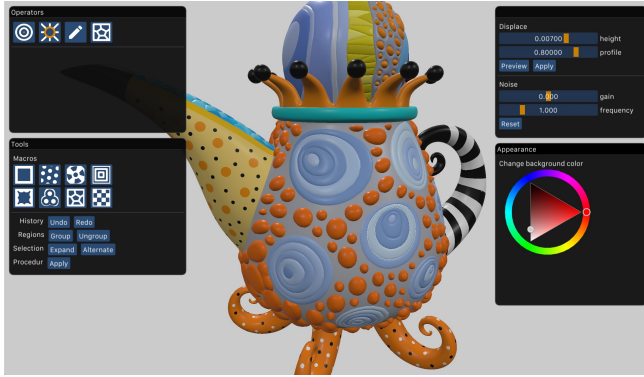


Fig. 8. We implemented an application for real-time editing that let the user decorate an input model applying the operators described in Sec. 3.2 directly. The user interface also features utilities for all the operations described in Sec. 3, such as surface displacement, perturbation, macros and procedural pattern generation.

Finally, we allow the user to apply arbitrarily-large surface displacement, after each operator is applied. The displacement is proportional to the geodesic distance from the region boundaries, being null at the boundaries to avoid discontinuities. Its profile is controlled by applying gain and bias operators from [29], to create bumps, pits, ridges or spikes. This feature has been used extensively in most of our results, see Figures 1, 10 and 12.

3.4 User Interface

To create and edit decorative patterns, we have implemented a user interface that presents to the user the selection methods and split operators exactly as described previously. We choose to use a straightforward mapping of the operators’ types and parameters to the interface since we found it easy to manipulate them directly, without further remapping or interface tuning. To further simplify editing, we support hierarchy tree navigation and undo, respectively by maintaining the pattern hierarchy and by storing snapshots of the internal data structures. Fig. 8 shows the user interface that is also demonstrated in the supplemental video. We have used this interface to generate all results in this paper.

Macros. Overall we found that by combining selection, operators and hierarchy we can create very complex patterns with ease. We also found that some specific combinations of operators and seed sets were often chosen together to create distinctive and recognizable patterns. To reduce manual work, we bundle these configurations into “macros”, in a manner similar to 3D editors. In our application, each macro is represented with just a button in the interface. Fig. 9 shows two simple sequences of editing using the eight macros we found most useful. See figure caption for a description.

Feedback Cycle. Applying an operator always implies first computing a geodesic field and then cutting the surface along its contour lines or integral curves. We show live previews of the final result before cutting the mesh, by just coloring the surface with real-time shaders. This gives immediate, meaningful and precise feedback

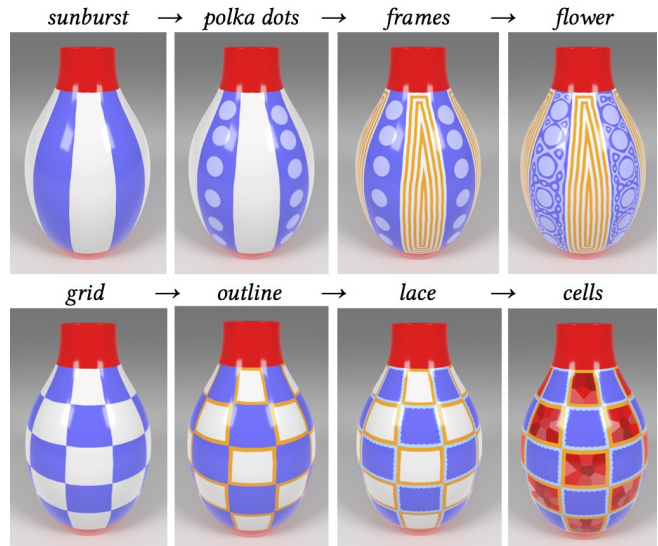


Fig. 9. Example decoration created by applying four macros successively. (First row, left to right): Example decoration applying four macros successively. (1) The *sunburst* macro creates longitudinal stripes or wedges connecting the two borders of a cylindrical region, by applying the *stream* operator and the two boundaries as seed sets. (2) The *polka dots* macro, in the blue region, creates dots by applying the *contour* operator to a set of Poisson-sampled seed points from the selected region. (3) The *frames* macro generates concentric outlines by applying the *contour* operator recursively to the boundary of the selected region, that in this case is the white one. (4) The *flower* macro creates flowing decorations by applying the *contour* operator to the *blend* between the distance from the region boundaries and the distance from Poisson-sampled points. (Second row from the left) Example decoration created by applying four macros successively. (5) The *grid* macro generates checkerboards by recursively applying the *contour* and *stream* operators between the opposite boundaries of a cylindrical region. (6) The *outline* macro creates outlines by applying the *contour* operator to all the boundaries off the selected boundaries. (7) The *lace* macro create embroidery-like decorations by applying the *contour* operator to seed points uniformly sampled from the boundaries of the selected region. (8) The *cells* macro creates cellular patterns by applying the *Voronoi* operator to Poisson-sampled seed points.

before actually modifying the model. In turn, this allows the user to work non-destructively while seeking good parameter values, and only commit the edit once it is good.

3.5 Procedural Patterns

The operators described before can also be applied automatically to generate fully procedural patterns. [28] demonstrate how to generate 2D recursive patterns using group grammars, a variation of context-free grammars that can be used to describe stochastic recursive patterns. While our operators and selections are very different from theirs, the manner in which they can be recursively applied is similar. Inspired by their work, we have implemented procedural patterns as described below using a formalism which is equivalent to a group grammar. In contrast to prior work, we integrate procedural generation in our interface, where procedural expansion



Fig. 10. Examples of fully procedural decorations created automatically (except colors). Procedural patterns are created by recursively applying macros that are sampled stochastically. After each expansion, regions are regrouped as in [28], to achieve more structured results. The composability of our operators guarantees that procedural generation is always robust and can be applied at any point of the editing session.

can be applied to any region by just clicking a button. The resulting pattern can then be non-destructively edited interactively. The user controls procedural generation just by selecting the region to edit, unlike [28] that require users to edit grammars directly. We follow a simpler approach since we focus on interactive editing and not grammar definitions, which are notoriously hard to edit, especially for designers. The resulting generator is equivalent to one example instance of group grammars, demonstrating that our operators and selections can also be controlled procedurally if desired.

Procedural Generation. We generate procedural patterns by recursively applying macros with default parameters to the leaf regions of the pattern tree. For each region, the macro to be applied is sampled stochastically, with a probability that depends on specific attributes of the region. Region attributes describe its overall shape as well as the way it was generated, and determine which macro would probably generate a pleasing result. The selection tags and probabilities used for our patterns are included in the supplemental material. Here we describe the features we use to derive them.

For each region, we keep track of its boundary loops and corners, namely the intersection points where three or more regions meet. For example, a region with one boundary and four corners will likely produce pleasing grid patterns. This is akin to [28] where they instead track directionality of shapes, which is hard to do on surfaces since absolute tangent directions cannot be defined in a coherent manner.

As in group grammars, each region is assigned a type tag depending on the kind of operation that generated it and the number of region corners. For example, after an *outline*, we differentiate regions between the inside and the border band, and after *dots*, we differentiate the circle-shaped regions from the background. After each expansion, regions are grouped with the same rules used in [28], so that the same macro is then applied to each region of a group, to obtain more structured results. Some examples of such rules are to group regions by type, by attributes or with a cyclic rule to obtain alternating or checked patterns. Procedural displacement is applied uniformly after the expansion is complete, while the choice of colors and materials is left to the user.

Discussion. Fig. 10 shows example patterns generated procedurally. These examples show that operators and selections can be

controlled procedurally. The main reason is that the operators can be applied to most regions independently of the region shape, i.e. they are closed under composition. This means that we can apply them recursively at will, which in turn implies that we can use many procedural formulations introduced by prior work to control the generation of procedurals recursive details directly on surfaces.

4 IMPLEMENTATION

In the discrete setting we encode the manifold \mathcal{M} as a finely tessellated triangle mesh M . We refine the mesh after applying each operator to precisely embed region boundaries as chains of edges, allowing us to represent regions exactly as groups of triangles. Since we target design applications, we support real-time interaction on commodity hardware on meshes up to a few million triangles.

Our implementation relies on geodesic distance fields, which are notoriously expensive to compute, especially for large meshes. We use a simple graph-based geodesic solver that is efficient, scalable, accurate enough at our tessellation level, and easy to update as the mesh is refined and displaced. We achieve efficiency and scalability by encoding the mesh and the graph with compact and tightly coupled data structures. This data-oriented design has other benefits since it easily supports undos, serialization and rendering; we will not discuss these aspects in this paper, though.

In the remainder of this section, we discuss implementation details to aid in reproducibility. We will also release an open-source implementation upon paper acceptance.

4.1 Representation

Mesh data structure. We encode triangle meshes with an indexed data structure augmented with face adjacencies, a.k.a. winged data structure [26], compactly stored in three arrays: positions (`float[3]`), triangles (`int[3]`), and face adjacencies (`int[3]`). The indexed format provides a minimal representation of geometry and connectivity, while adjacencies provide support for efficient line tracing, region flooding and boundary computation.

Pattern representation. Our patterns partition the surface into regions. We represent regions implicitly by labeling each triangle with the identifier of the region containing it. Hence, the collection of patterns covering the mesh is represented as an array of integers,

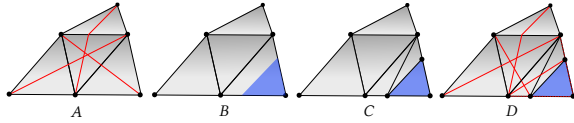


Fig. 11. (A) Our graph has one node for each vertex in the mesh (black dots), a bidirectional arc for each edge in the mesh (black lines) and for each pair of vertices that are opposite to an edge (red lines). The weight of each arc is equal to the geodesic distance between the connected vertices. (B) When an operator is applied, the surface is partitioned into new regions (blue and grey). The boundary that separates the new regions is a polyline crossing the edges of the triangles in the mesh. (C) The mesh is refined to embed the polyline, so that each triangle belongs to one region. (D) Only arcs in the graph traversing the split triangles are updated.

one for each triangle. We maintain the hierarchy of region tags in a tree data structure, with a negligible space overhead, as it contains at most few thousands nodes even on our most complex results, as shown in Fig. 13. Compared to storing a hierarchy of meshes, this separate representation is both significantly more compact and does not need to be updated as the mesh is refined.

Field representation. Scalar fields are encoded at mesh vertices and extended by linear interpolation, while their gradient field is piecewise-constant on triangles. Operators compute either contour lines or integral curves, including geodesic paths, which cut the mesh along polylines. We split all triangles intersected by such polylines every time an operator is applied, so that regions always consist of discrete collections of triangles.

4.2 Geodesic Computations

Geodesic Graph. Our solver is implemented using the graph exemplified in Fig. 11. Nodes correspond to mesh vertices, while arcs correspond to mesh edges as well as dual edges, i.e., arcs connecting pairs of vertices opposite to an edge. The length of each arc is computed as the exact geodesic distance between the vertices it connects. Arc lengths are stored in single precision to reduce memory usage, as our method is not prone to high error propagation – distances are just summed during graph visit – while most approximation error stems from discretizing geodesic paths along arcs of the graph.

We store the graph as adjacency lists with a simple array of arrays data structure, where we employ small vector optimizations for the adjacency lists. This solution ensures that most of the graph is laid-out on a single contiguous chunk of data, which reduces heap pressure and improves cache locality during the graph visit.

We build the graph once at the beginning of the editing session, by using face adjacencies to construct dual edges, as shown in the supplemental pseudocode. Then we *locally* update the graph after each mesh refinement operation: updates only involve nodes incident at split triangles, which are retrieved easily and efficiently, thanks to the implicit connection between vertices and nodes, and edges/adjacencies and arcs. Updates upon displacement are also efficient since they only require recomputing edge lengths, without modifying the graph topology.

Geodesic Solve. We compute geodesic distance fields by wavefront expansion over the graph, shown as pseudocode in supplemental. We adopt the small-label-first (SLF) and large-label-last (LLL) heuristics [1], which do not require a priority queue. These techniques perform significantly faster than classical Dijkstra search on this kind of graphs [33]. Our implementation aggressively exploits computation locality, by applying early exits when bounding the graph search to a region. The general solver computes distance fields from any given set of vertices. Seed sets corresponding to lines are just sampled at their vertices. Note that we use our solver just to compute the geodesic distance, while we do not trace geodesic paths with sequences of arcs in the graph, as the latter would result in wiggly polylines.

Poisson sampling. We use Poisson sampling to generate seed sets for various operators. We adopt a farthest point sampling technique [13] under the geodesic metric. This scheme requires the computation of a distance field for each sampling point, which may become expensive as many points are sampled over large regions. We take advantage of the wavefront nature of graph search to significantly optimize the computation time.

We begin by computing the distance field from the region boundary. Then we iteratively select the vertex with maximum distance and add it to the seed set, and we update the distance field by expanding from the new seed, without resetting the already computed distances. This allows us to update the distance field only in the proximity of the new seed, by exploiting early exit when hitting nodes that already have a shorter distance from the previous set. The search radius becomes increasingly smaller as points are added to the seed set, resulting in a significant speedup. See statistics in the supplemental material. This is another advantage of a graph-based solver over alternatives that are non-local.

Line tracing. Operators require extracting contour lines and integral curves, as well as cutting the mesh with such lines. Contour lines are extracted per triangle by linear interpolation. Integral curves and geodesic paths are computed by tracing the piecewise-constant gradient per triangle. Each triangle intersected by one such line is split along the corresponding segment, forming three new triangles. When a triangle is split, arcs and nodes are added to the graph to represent new vertices and edges, and the adjacency of nodes in the split triangle is updated accordingly, as shown in Fig. 11.

Operators. The operators described in Sec. 3 are implemented on top of the functionality described before. The *contour* operator requires one or two geodesic solves, for *dist* and *blend* respectively, followed by the extraction of isolines and cuts along them. The *stream* operator requires the same solves, this time followed by cuts along integral curves. In both cases, computation is bound to the region in which the operator is applied.

The *polyline* operator is implemented by tracing geodesic paths between each pair of successive points. Each segment is computed starting at a vertex and ascending the gradient of the distance field generated from the previous vertex. This operation requires one solve per segment: early exit occurs as soon as the target vertex is reached, so computation is bound to the intersection between the selected region and a geodesic circle having the segment as radius.

The *Voronoi* operator requires a solve for each element in the seed set, which may become expensive for large seed sets. We again optimize this operator by exploiting early exits in graph search. We first compute the distance field from all seeds together to find its maximum value. We then set this distance as bound for early exit when computing the field for each seed. Intuitively, this ensures that each mesh vertex is visited roughly twice, so computation time is bounded regardless of the number of seeds. For each vertex of the region of interest, we collect the distance from its three closest seeds. Then we generate the Voronoi diagram by splitting all triangles that have vertices lying in different Voronoi regions, as in [16]. See statistics in the supplemental material for time performance.

Finally, shape perturbation and displacement are trivially implemented by updating the edge lengths in the graph, and the positions of vertices, respectively.

Discussion. Our system is very compact and coherent, because all operations rely on geodesic distance computation, as well as on few other straightforward operations: line tracing and mesh cutting. Performance depends on our capability to make geodesic computations fast, and update our data structures efficiently. In this sense, the choice of our specific graph solver provides an optimal tradeoff under a variety of aspects, such as accuracy, speed, scalability, simplicity, dynamic update, and early exits. Scalability, simplicity and ease of update descend from using just the vertices of the mesh as nodes, and relations from local mesh topology as arcs. Nodes in our graph have average degree of 12, hence for a mesh with N vertices our graph has N nodes and about $6N$ bidirectional arcs.

In contrast, graph-based methods using Steiner nodes [19, 20] are much more complex to maintain upon dynamic updates, and have a larger memory footprint. Their number of arcs increases quadratically with the number k of Steiner nodes per edge: for $k = 1$ there are $\sim 4N$ nodes and $\sim 18N$ arcs; while, for $k = 3$, the count raises to $\sim 10N$ nodes and $\sim 84N$ arcs, making these graphs impractical for large meshes even with moderately low values of k .

The DGG [33] and SVG [35] methods use graphs that do have just the vertices as nodes, but each node has a high degree (order $10^2 - 10^3$). Their memory footprint is high and they are slow to update upon mesh refinement. Finally, the method proposed in [4] relies just on the graph of edges, but computations to straighten paths are done on-the-fly, making the method suitable for point-to-point path computation only.

With the PDE method of [8], each solve implies the solution of a sparse $N \times N$ linear system, which can be pre-factorized for a given mesh, making the solution fast at the price of pre-computation. The main concern in using this method is that every time we change the mesh topology or geometry the expensive factorization step needs to be repeated. See Sec. 5.2 for a comparative analysis in terms of accuracy and performance.

5 RESULTS AND VALIDATION

We validated our pattern model in three manners. First, we modeled decorations that match real-world styles. Second, we tested the accuracy and speed of the overall system and of the geodesic solver to show that it remains interactive. Third, we validated our user

interface with a user study to show that novices to the system can replicate given patterns.

5.1 Editing Sequences

Fig. 1 and Fig. 12 show complex patterns created with our system during interactive sessions. We chose to model patterns from real-world examples with different artistic styles to show that our model can capture intricate decorations made by artisans. Fig. 13 shows statistics of the editing sequences corresponding to such images.

Overall we found that creating complex patterns is easy with our interface. We used from up to hundreds of single operations to create patterns made of up to 1800 individual decorations, which correspond to regions in our model. Note that some such operations were applied as macros or procedurals, simplifying editing further. The number of operations we employ is significantly smaller than using standard modeling tools with either polygonal modeling or sculpting workflows, e.g. see [10, 11] for statistics of common modeling sequences.

To gain a better sense of the recursive nature of the decorations, we report the depth of the pattern tree, which reached 21 in our most intricate result. This shows that by applying patterns recursively, even just a few times, we can greatly increase the complexity of the decoration while maintaining the editing manageable for users.

5.2 Performance and Accuracy

In our examples, we handle models between 500k and 2M triangles, which are further subdivided during editing. Throughout the modeling sequences, our system remains interactive with computation times of about 0.2s per operation, including geodesic computation, mesh cutting and graph update. Memory usage is also compact, never exceeding 300Mb, which includes the mesh and the geodesic solver, as well as interface support data. Performances were evaluated on a 2.9 GHz laptop with 16 GB of RAM running with a single-core for our application.

Fast geodesic computation is the main technical feature that enables us to model decorations well. We test the performance and accuracy of our solver by computing the geodesic field from a single source to all vertices on a variety of meshes, summarized in Fig. 14. While we use a very simple graph, our solver remains accurate enough with an error between 1.1% and 1.6% over a state of the art solver for exact polyhedral geodesics [27]. Computation times are between 0.015s and 0.446s for a single core implementation running on meshes between 300k and 7.2M triangles. This speed is fast enough for all our modeling needs.

We compared our solver to a popular, approximate, geodesic solver based on PDEs [8] using the author’s implementation. The accuracy of our solver is just slightly lower on relatively small meshes, while getting better on large meshes. On the other hand, our solver consistently runs at roughly twice the speed, always remaining compatible with interaction, even when considering the additional times for update after mesh cutting.

In terms of pre-computation times, where [8] factorize a sparse matrix, while we build a graph, our method runs roughly between 10 and 35 times faster. Although pre-computation is just performed



Fig. 12. Results created with our application starting from undecorated models, shown in the insets. Decorations were inspired by real world examples: the tank-teapot on the left reproduces the playful look of handmade toys, the result in the middle matches the appearance of carnival masks of Venice, the statue on the right is decorated with intricate patterns that imitate tangles on ceramics. Statistics about the models and the editing sessions are reported in Fig. 13

model name	triangles at start	triangles at end	number of regions	number of operations	tree depth	average time per operation	memory usage at end
fertility	0.50M	0.90M	1810	655	21	0.134s	96Mb
teapot	1.50M	1.65M	511	129	13	0.146s	173Mb
tank	1.45M	1.68M	636	145	10	0.189s	174Mb
mask	2.00M	2.15M	62	30	5	0.232s	228Mb
elephant	2.00M	2.61M	364	212	13	0.241s	278Mb

Fig. 13. Statistics on the editing sequences used for interactive decoration. The average time per operation takes into account the time needed to compute the geodesic field, cut the mesh, update the graph and the pattern representation data.

model name	triangles	[27]		[8]			ours			
		solve	build	solve	error	build	solve	error	update	
kitten	300k	3.0s	1.49s	0.068s	0.5%	0.061s (24x)	0.015s (4.5x)	1.1%	0.013s	
elephant	500k	10.9s	3.47s	0.095s	0.5%	0.098s (35x)	0.027s (3.5x)	1.1%	0.023s	
fertility	500k	3.5s	2.86s	0.123s	0.5%	0.109s (26x)	0.026s (4.8x)	1.1%	0.023s	
lucy	525k	9.1s	1.98s	0.082s	1.5%	0.175s (11x)	0.034s (2.4x)	1.6%	0.025s	
mask	2.0M	121.0s	14.4s	0.391s	1.1%	0.585s (24x)	0.114s (3.4x)	1.2%	0.115s	
nefertiti	2.0M	20.3s	14.8s	0.345s	0.9%	0.730s (20x)	0.149s (2.3x)	1.5%	0.139s	
dragon	7.2M	79.9s	59.6s	1.500s	3.0%	2.613s (24x)	0.446s (3.9x)	1.5%	0.571s	

Fig. 14. Comparison between our geodesic solver, and the solver from [8]. For the latter we use the implementation provided by the author, using Cholmod as backend. Columns *build* report pre-processing times to pre-factor the system and to build the graph, respectively. Build times for our solver also include the time to compute the triangle adjacency needed to build the graph. Columns *solve* report average time for computing the distance field from a single point source, where average is taken over 100 random samples. Column *update* reports the average time to update our graph after mesh split, where average is taken over 100 different long slices that roughly cut the mesh in half. Root-mean-square errors are computed with respect to the exact polyhedral solution from [27].

once, the high times of [8] suggest that it would be hard to try a dynamic update after mesh edit.

We also compared our solver to a straightforward implementation of Lanthier’s graph [20] with just one Steiner point per edge, using the same graph traversal algorithm. In terms of accuracy, results are comparable to our solver. We cannot objectively compare solve times as the two implementations were not equally optimized, but

on average our solver was about 10 times faster. Regardless of low-level optimizations, we assume our method to be more efficient, as the Lanthier’s graph with one Steiner node per edge is more than three times larger, as explained in Sec. 4.2. Beyond accuracy and performance, our graph is much easier to maintain upon mesh cutting, and that was the determining factor, which made it a better choice for our application.

We wish to remark that the choice of a geodesic solver is relatively orthogonal to our pattern model, though.

5.3 User Study

We ran a user study to validate whether our prototype system is easy to use, whether it allows users to model complex patterns, and whether the style of the models we produce matches the style found in handmade artisanal objects.

Experimental procedure. We asked 17 subjects with different degrees of expertise, ranging from novices to professional 3D artists, to use our prototype after a short training and an unguided editing session on a model of their choice. We asked subjects to perform three matching tasks of increasing difficulty, in which they had to use the application to reproduce a target image shown in a picture. Images are provided in the additional material and in Fig. 15.

After each task, subjects were asked to rate the similarity of their result with the reference and to evaluate how easy they found it to complete the task, using a scale from 1 to 10. We also asked subjects to rate whether they would have been able to obtain the same kind of results with a different 3D application, whether they found the interface responsive, and whether they were satisfied with the overall experience. Finally, we have shown to the subjects the teapot and the elephant decorated models from Fig. 1, and asked them to recognize whether the style of the image matches real photographs of similar styles, compared to other alternatives. We include a copy of the final questionnaire in the supplemental material.

Quantitative Evaluation. Fig. 15 shows the results of our user study, where for all ratings we rejected the null hypothesis ($p \leq 0.05$), i.e. those results are statistically significant.

All 17 users were able to successfully complete the reproduction tasks, spending different amounts of time in the editing session, but never more than 4 minutes for each task, out of a maximum task length of 5 minutes. All users rated their results quite similar, if not identical, to the reference ones. This suggests that our interface provides sufficient control to reproduce given complex patterns. All subjects also found the tasks easy to perform, and reported that they would not have been able to obtain the same kind of results with a different 3D editing software.

In general, all subjects also found the interface responsive and were satisfied with the overall experience with the application, confirming that our implementation remains interactive at all times. All subjects but one correctly recognized the style from which our results were inspired, meaning that the models produced by our application match the look of real hand-crafted objects.

In conclusion, the user study demonstrated that users agree that our application is expressive, easy to use, and can produce results that match the look of real decorated objects.

Qualitative Feedback. Some non-expert users informally reported that they were surprised by the complexity of the results they managed to obtain with the application and the ease with which they were able to control the editing operations. We think that this cannot be explained only by the usability of the interface, but rather it is a direct consequence of the intuitive design of our editing operators, which requires no expertise to be understood. These facts

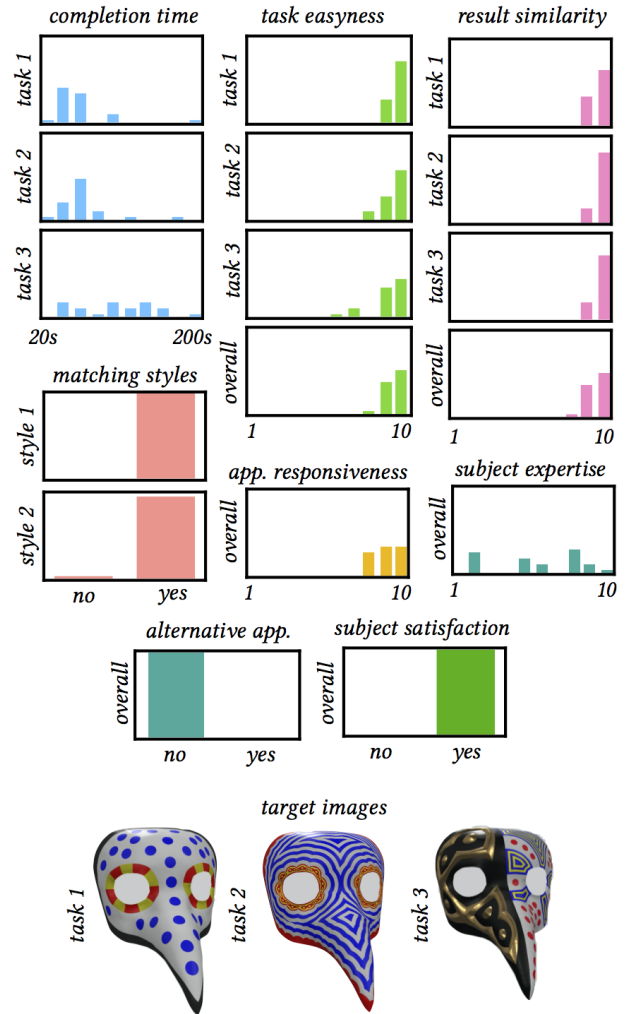


Fig. 15. Result data from the user study. Histograms on the left report the time spent by the subjects to complete each task. The bar chart just below shows that all subjects but one correctly recognized the real world styles from which our results in Fig. 1 were inspired. The remaining bar charts show subjects’ feedback about their tasks: users with different amount of expertise found the tasks easy to perform, their results similar to the reference ones and the application responsive. All subjects were satisfied with their editing experience with the application and do not think that using another digital tool would allow them to obtain the same results in the same time.

suggest that the editing workflow of our application is well-suited for non-technical artists and designers, too.

Experts users reported that they found the application responsive and pleasant to use. We quote here some informal feedback we collected: “The editing was surprisingly fast and enjoyable. I did not have to think about triangles, edge loops or topology issues as in Maya or Blender; I could just focus on the result.”

5.4 Limitations

Patterns. While we introduce a general pattern model, recursive patterns based on tight packing of arbitrarily-shaped elements cannot be easily reproduced in terms of geodesics. While there is a large literature on this, we remind the reader that packing is NP-hard in general, so all methods proposed so far are necessarily strong approximations.

Another type of pattern that we did not specifically include is floral decorations. One possibility would be to adapt a region-growing model similar to the one used in procedural trees and express it in terms of geodesic paths. The main concern though is that controlling floral arrangement over an arbitrary manifold remains hard since there is no global orientation to use while growing. We leave the investigation of such further patterns to future work.

Discretization. We rely on fine tessellations to represent decorations and discretize geodesic computation. Using too few triangles may introduce artifacts, such as wiggly polylines, due to mesh discretization, graph-based evaluation of distance fields and piecewise-constant approximation of gradient fields. While we did not witness these problems in our tests, they are nonetheless possible. An alternative would be to separate the modeling and rendering phases. Since all our decorations can be encoded as operations on the manifold and its sub-regions, final patterns can be regenerated before rendering. This would allow us to use an accurate representation of the manifold, such as a more refined mesh or a subdivision surface, more accurate geodesy, such as exact methods for meshes or PDE methods for subdivision surfaces [9], and more accurate methods for isoline extraction and vector field tracing [18, 24].

6 CONCLUDING REMARKS

We have presented an interactive method for generating recursive patterns on surfaces and its use to model real-world decorations. Our model consists of a closed algebra of regions, which can be split by applying four operators at will. Operators are defined upon geodesic fields on the surface and our implementation relies on fast geodesic computations. A user study shows that the resulting application is effective, it is responsive on meshes in the order of one or a few million triangles, and it is easy to use for novices too.

Our system is easily extensible in a variety of ways. Directional fields [32] can be used to generate patterns based on further streamlines, which can be easily combed and constrained to lines and boundaries in the decor. Fields can be also used to locally parameterize patches of the surface, thus allowing for a mixed use of our vector graphics together with raster graphics, i.e. textures, to create a composite decor. Diffusion curves [25] can be naturally incorporated too, to support smooth-shaded coloring of regions.

REFERENCES

- [1] Dimitri P. Bertsekas. 1998. *Network optimization: continuous and discrete models*. Athena Scientific.
- [2] Prosenjit Bose, Anil Maheshwari, Chang Shu, and Stefanie Wuhler. 2011. A Survey of Geodesic Paths on 3D Surfaces. *Comput. Geom. Theory Appl.* 44, 9 (2011), 486–498.
- [3] Luciano A. Romero Calla, Lizeth J. Fuentes Perez, and Anselmo A. Montenegro. 2019. A minimalistic approach for fast computation of geodesic distances on triangular meshes. *Computers & Graphics* 84 (2019), 77 – 92.
- [4] Marcel Campen, Martin Heistermann, and Leif Kobbelt. 2013. Practical Anisotropic Geodesy. In *Proc. Symposium on Geometry Processing*. 63–71.
- [5] Marcel Campen and Leif Kobbelt. 2011. Walking On Broken Mesh: Defect-Tolerant Geodesic Distances and Parameterizations. *Eurographics* 30 (2011), Issue 2.
- [6] Edoardo Carra, Christian Santoni, and Fabio Pellacini. 2019. Grammar-based procedural animations for motion graphics. *Computers & Graphics* 78 (2019), 97–107.
- [7] Jindong Chen and Yijie Han. 1990. Shortest Paths on a Polyhedron. In *Proc. Symposium on Computational Geometry (SCG '90)*. 360–369.
- [8] Keenan Crane, Clarisse Weischedel, and Max Wardetzky. 2013. Geodesics in heat: A new approach to computing distance based on heat flow. *ACM Trans. Graph.* 32, 5 (2013).
- [9] Fernando De Goes, Mathieu Desbrun, Mark Meyer, and Tony DeRose. 2016. Subdivision exterior calculus for geometry processing. *ACM Trans. Graph.* 35, 4 (2016).
- [10] Jonathan D. Denning, William B. Kerr, and Fabio Pellacini. 2011. MeshFlow: Interactive Visualization of Mesh Construction Sequences. *ACM Trans. Graph.* 30, 4 (2011).
- [11] Jonathan D. Denning, Valentina Tibaldo, and Fabio Pellacini. 2015. 3DFlow: Continuous Summarization of Mesh Editing Workflows. *ACM Trans. Graph.* 34, 4 (2015).
- [12] David Ebert, Kenton Musgrave, Darwyn Peachey, Ken Perlin, and Steve Worley. 2002. *Texturing and Modeling: A Procedural Approach* (3 ed.). Morgan Kaufmann.
- [13] Y. Eldar, M. Lindenbaum, M. Porat, and Y. Y. Zeevi. 1997. The Farthest Point Strategy for Progressive Image Sampling. *Trans. Img. Proc.* 6, 9 (1997).
- [14] Philipp Herholz and Marc Alexa. 2018. Factor once: Reusing cholesky factorizations on sub-meshes. *ACM Trans. Graph.* 37 (2018).
- [15] Philipp Herholz, Timothy A. Davis, and Marc Alexa. 2017. Localized Solutions of Sparse Linear Systems for Geometry Processing. *ACM Trans. Graph.* 36, 6 (2017).
- [16] Philipp Herholz, Felix Haase, and Marc Alexa. 2017. Diffusion diagrams: Voronoi cells and centroids from diffusion. In *Computer Graphics Forum*, Vol. 36. Wiley Online Library, 163–175.
- [17] R. Kimmel and J. A. Sethian. 1998. Computing Geodesic Paths on Manifolds. In *Proc. Natl. Acad. Sci. USA*. 8431–8435.
- [18] Peter Kipfer, Frank Reck, and Günther Greiner. 2003. Local exact particle tracing on unstructured grids. *Computer Graphics Forum* 22 (2003), 133–142.
- [19] Mark Lanthier, Anil Maheshwari, and Jörg-Rüdiger Sack. 1997. Approximating weighted shortest paths on polyhedral surfaces. In *Proc. of ACM Symposium on Computational Geometry*.
- [20] Mark Lanthier, Anil Maheshwari, and Jörg-Rüdiger Sack. 2001. Approximating shortest paths on weighted polyhedral surfaces. *Algorithmica* 30, 4 (2001), 527–562.
- [21] Yuanyuan Li, Fan Bao, Eugene Zhang, Yoshihiro Kobayashi, and Peter Wonka. 2011. Geometry Synthesis on Surfaces Using Field-Guided Shape Grammars. *IEEE Trans. Visualization and Computer Graphics* 17, 2 (2011).
- [22] Hugo Loi, Thomas Hurtut, Romain Vergne, and Joelle Thollot. 2017. Programmable 2D Arrangements for Element Texture Design. *ACM Trans. Graph.* 36, 3 (2017).
- [23] Joseph S. B. Mitchell, David M. Mount, and Christos H. Papadimitriou. 1987. The Discrete Geodesic Problem. *SIAM J. Comput.* 16, 4 (Aug. 1987), 647–668.
- [24] G. M. Nielson and Il-Hong Jung. 1999. Tools for computing tangent curves for linearly varying vector fields over tetrahedral domains. *IEEE Trans. Visualization and Computer Graphics* 5, 4 (1999), 360–372.
- [25] Alexandrina Orzan, Adrien Bousseau, Holger Winnemöller, Pascal Barla, Joëlle Thollot, and David Salesin. 2008. Diffusion Curves: A Vector Representation for Smooth-shaded Images. *ACM Trans. Graph.* 27, 3 (Aug. 2008), 92:1–92:8.
- [26] A. Paoluzzi, F. Bernardini, C. Cattani, and V. Ferrucci. 1993. Dimension-Independent Modeling with Simplicial Complexes. *ACM Trans. Graph.* 12, 1 (1993), 56–102.
- [27] Yipeng Qin, Xiaoguang Han, Hongchuan Yu, Yizhou Yu, and Jianjun Zhang. 2016. Fast and Exact Discrete Geodesic Computation Based on Triangle-oriented Wavefront Propagation. *ACM Trans. Graph.* 35, 4 (2016), 125:1–125:13.
- [28] Christian Santoni and Fabio Pellacini. 2016. gTangle: A Grammar for the Procedural Generation of Tangle Patterns. *ACM Trans. Graph.* 35, 6 (2016).
- [29] Christophe Schlick. 1994. Fast Alternatives to Perlin’s Bias and Gain Functions. *Graphics Gems IV* (1994).
- [30] Michael Schwarz and Peter Wonka. 2015. Practical Grammar-based Procedural Modeling of Architecture. In *SIGGRAPH Asia 2015 Courses*.
- [31] Omry Sendik and Daniel Cohen-Or. 2017. Deep Correlations for Texture Synthesis. *ACM Trans. Graph.* 36, 4, Article 105b (July 2017).
- [32] Amir Vaxman, Marcel Campen, Olga Diamanti, David Bommes, Klaus Hildebrandt, Mirela Ben-Chen Technion, and Daniele Panozzo. 2017. Directional Field Synthesis, Design, and Processing. In *ACM SIGGRAPH 2017 Courses*.
- [33] Xiaoning Wang, Zheng Fang, Jiajun Wu, Shi-Qing Xin, and Ying He. 2017. Discrete Geodesic Graph (DGG) for Computing Geodesic Distances on Polyhedral Surfaces. *Comput. Aided Geom. Des.* 52, C (2017), 262–284.

- [34] Li-Yi Wei, Sylvain Lefebvre, Vivek Kwatra, and Greg Turk. 2009. State of the Art in Example-based Texture Synthesis. In *Eurographics State of the Art Report*.
- [35] Xiang Ying, Xiaoning Wang, and Ying He. 2013. Saddle Vertex Graph (SVG): A Novel Solution to the Discrete Geodesic Problem. *ACM Trans. Graph.* 32, 6 (2013).
- [36] Yang Zhou, Zhen Zhu, Xiang Bai, Dani Lischinski, Daniel Cohen-Or, and Hui Huang. 2018. Non-stationary Texture Synthesis by Adversarial Expansion. *ACM Trans. Graph.* 37, 4 (2018).